RESEARCH ARTICLE

MATERIALS SCIENCE

Boosting molecular diffusion following the generalized Murray's Law by constructing hierarchical zeolites for maximized catalytic activity

Ming-Hui Sun[1,2,†], Shu-Shu Gao[3,5,†], Zhi-Yi Hu[1,4], Tarek Barakat[2], Zhan Liu,[1] Shen Yu,[1] Jia-Min Lyu,[1] Yu Li,[1] Shu-Tao Xu[5], Li-Hua Chen[1,*] and Bao-Lian Su[1,2,*]

[1]State Key Laboratory of Advanced Technology for Materials Synthesis and Processing, Wuhan University of Technology, Wuhan 430070, China;
[2]Laboratory of Inorganic Materials Chemistry (CMI), University of Namur, Namur B-5000, Belgium;
[3]Sinopec Beijing Research Institute of Chemical Industry, Beijing 100013, China;
[4]Nanostructure Research Centre, Wuhan University of Technology, Wuhan 430070, China;
[5]National Engineering Laboratory for Methanol to Olefins, Dalian National Laboratory for Clean Energy, Dalian Institute of Chemical Physics, Chinese Academy of Sciences, Dalian 116023, China
***Corresponding authors**. E-mails: chenlihua@whut.edu.cn; bao-lian.su@unamur.be

†Equally contributed to this work.

ABSTRACT

Diffusion is an extremely critical step in zeolite catalysis which determines the catalytic performance, in particular for the conversion of bulky molecules. Introducing interconnected mesopores and macropores into a single microporous zeolite with the rationalized pore size at each level is an effective strategy to suppress the diffusion limitations, but remains highly challenging due to the lack of rational design principles. Herein, we demonstrate the first example of boosting molecular diffusion by constructing hierarchical Murray zeolites with highly ordered and fully interconnected

1

ORIGINAL UNEDITED MANUSCRIPT

macro-meso-microporous structure on the basis of the generalized Murray's Law. Such hierarchical Murray zeolite with a refined quantitative relationship between pore size at each length scale exhibited 9 and 5 times higher effective diffusion rate, leading to 2.5 and 1.5 times higher catalytic performance in the bulky 1,3,5-triisopropylbenzene cracking reaction than those of microporous ZSM-5 and ZSM-5 nanocrystals, respectively. The concept of hierarchical Murray zeolites with optimized structural feature and their design principles could be applied to other catalytic reactions for maximized performance.

Keywords: Zeolites, hierarchically Murray structure, ordered porous hierarchy, generalized Murray's Law, catalytic cracking

INTRODUCTION

Diffusion, the decisive factor of mass transfer in microporous zeolite catalysts, is of crucial importance for their industrial utilization in catalysis, since the molecular mobility is a rate-limiting step of the overall catalyzed reaction processes[1-3]. However, the diffusion of molecules in the micropores (the configurational diffusion) is at least one order of magnitude lower than those in mesopores (the Knudsen-diffusion) and macropores (the molecular-diffusion) [4]. Such low diffusivities in micropores lead to restricted access and delayed transport of molecules to/from the catalytically active site constrained within micropores, resulting in short catalyst lifetime and poor zeolite utilization[5-7]. Introducing additional mesopores or/and macropores into the microporous zeolites offer an effective solution to enhance

2

the mass transportation property for improved catalytic performance[2,5,8-20]. Kärger et al prepared nanosheet assemblies of zeolite X with intracrystalline mesopores of 7 nm, which showed a cyclohexane diffusion enhancement by one order of magnitude and 3 times higher benzylchloride conversion in the benzylation of toluene compared to purely microporous sample[12]. Pérez-Ramírez et al synthesized mesoporous zeolite ZSM-5 by desilication, which exhibited a 6 times improved effective diffusivity of 2,2-dimethylbutane[13] and a 3.3 times extended cycle time in the conversion of methanol to olefin in comparison with traditional zeolites[14]. Our group reported an *in situ* bottom-up confined crystallization process to synthesize zeolite ZSM-5 single crystals with a fully interconnected and highly ordered intracrystalline macro-meso-microporosity[15]. Such hierarchically porous single crystal reactors provided a highly efficient diffusion system with the relative diffusion of bulky aromatic molecules 7 times higher and therefore a greatly improved catalytic performance with the lifetime 13 times longer than their microporous counterparts[15]. Most previously reported works on the synthesis of hierarchically porous zeolites lack the rational design principles. Additionally, most of the aforementioned hierarchical pores are often disordered and not uniform although it is clear that the introduction of meso-macropores into microporous zeolites can more or less improve the catalytic performance. Further comprehensive work is needed to clarify how to optimize the hierarchically porous structure with predicted and rationalized pore size at each level for a maximized catalytic performance[21-25].

Perez-Ramirez et al. proposed a Hierarchy Factor (HF) concept to design hierarchically

3

porous zeolites[26], which describes the ratio between the relative mesoporous surface area (S_{meso}/S_{BET}) and the relative micropore volume (V_{micro}/V_{pore}). Higher HF refers to better matching of micro- and mesoporosity, and therefore leads to better catalytic performance. This HF concept focuses on the impact of micropores and mesopores. Further introduction of the effect of macropores together with the interconnection between different level pores and the quantitative analysis will offer HF concept more power[26]. The evolution by natural selection creates various classes of hierarchically porous organisms, such as leaf veins, kidney, lung, vascular and respiratory systems for survival and productions[2]. In 1926, Murray proposed the first law to stipulate the rational relationship between pore radii ratio at each pore level. Murray's Law, using a biological consideration, is a general empirical principle of great utility in predicting porous parameters in the bulk transport systems for connecting large vessels to small. In spite of strong interests, Murray's ideas went almost unnoticed for nearly a century as this Law is based on the assumption of constant flow[27]. Recently, our group revisited the Murray's Law and established equation (Equation S1) referred to the generalized Murray's Law, which predict the precise diameter ratios for interconnected multi-scale pores from macroscopic to microscopic levels (Equations S2 and S3), for the quantitative design of optimized hierarchically porous materials by taking the mass variations and constant surface substance exchange during the mass transportations[28]. Following the generalized Murray's Law, hierarchically macro-meso-microporous ZnO materials (ZnO M-M-M) emulating the natural vascular structure were constructed and delivered a 2.5 times faster adsorption rate of rhodamine B than micro-mesoporous ZnO (ZnO M-M) in the photocatalytic degradation process[28]. With such Murray network architecture for fast mass diffusion and exchange in

4

the liquid-solid reaction, ZnO M-M-M shows 2.5 times higher photocatalytic acticivty than that of ZnO M-M. Similarly, ZnO-M-M-M also enable highly enhanced mass exchange and transfer in gas-solid and electrochemical reactions and exhibit enhanced 25- or 40-fold increases in performance compared to unimodal mesoporous materials performance in gas sensing and as Li-ion battery electrodes, respectively. This concept of 'learning from nature' offers inspiration in the quantitative design and synthesis of hierarchically porous materials with advanced performances. Regarding to the microporous structure of zeolites, the introduced macropores offer an unimpeded transport path while the introduced mesopores provide a fast pathway for mass transportation bridging the intrinsic micropores and the additional macropores[29]. Therefore, engineering the mesoporous and macroporous structure to match the zeolite micropores based on the generalized Murray's Law is essential to boost diffusion performances for maximized catalytic properties[30].

Herein, we demonstrate the proof of the concept of boosting molecular diffusion by constructing hierarchical Murray zeolites presenting highly ordered and fully interconnected macro-meso-microporous structure whose pore size ratio at each length scale is rationally modulated based on the generalized Murray's Law. For the first time, the generalized Murray's Law was used to establish the relationship between the structural characteristics, the diffusion behaviours and the catalytic performance in zeolite catalysis. Such hierarchically Murray zeolite catalyst exhibits excellent mass transport properties with an effective diffusion rate of bulky 1,3,5-trimethylbenzene 9 and 5 times higher together with 2.5 times and 1.5 times higher 1,3,5-triisopropylbenzene cracking conversions than purely microporous ZSM-5 and

5

ZSM-5 nanocrystals, respectively. The strategy presents in this work enables the predictable and controlled synthesis of hierarchically porous zeolites with a quantitative hierarchy for optimized structural features and maximized performance.

RESULTS AND DISCUSSIONS

The confined crystalline transformation process was adapted to synthesize hierarchical Murray zeolite with a highly interconnected and three-dimensionally ordered macro-mesoporous structure assembled by uniform zeolite nanocrystals. The monodisperse polystyrene microspheres were used as templates for the three-dimensional ordered macropores. The walls of macropores are constructed from the assembly of highly uniform zeolite nanocrystals, which leads to the formation of an interconnected ordered mesoporous system. The interparticular mesopore size is determined by the size of uniform zeolite nanocrystals. The detailed synthesis route is illustrated in Figure 1a. Firstly, the polystyrene spheres and the amorphous silica nanospheres (22 nm) were added into sucrose solution containing sulfuric acid to obtain stable dispersion (i in Figure 1a). Three dimensionally periodic close-packed polystyrene spheres/silica spheres (ii in Figure 1a) were obtained via an evaporation induced self-assembly method (Step 1 in Figure 1a), followed by a preliminary carbonization process (Step 2 in Figure 1a) to construct PS/SiO_2/carbon matrix. The PS/SiO_2/carbon matrix as both the zeolite silica precursors and macropore/mesopore template. The in-situ formed carbon in the PS/SiO_2/carbon matrix acted as a rigid supporting material to immobilize the three dimensionally ordered close-packed PS nanospheres and SiO_2

6

nanospheres and avoid the collapse of such ordered structure during the crystalline process. Moreover, the confinement effect of the carbon ensures that the final size of zeolite nanocrystals did not exceed the size of the original silica nanospheres (20 nm). This matrix was subsequently used as the zeolite silica precursors (iii in Figure 1a) and was infiltrated with tetrapropylammonium ion (TPA^+) and alumina source. TPA^+ and alumina permeated into the matrix evenly by a vacuum-rotary evaporation process. After sealing in a Teflon-lined stainless-steel autoclave, the amorphous silica spheres located in the PS/SiO_2/carbon matrix gradually *in-situ* reacted with aluminium precursor and crystallized around the structure directing agents TPA^+ within the confined space during hydrothermal process (Step 3 in Figure 1a). The silica nanoparticles, located in the macropore walls and interstitials, transformed completely to zeolite crystals (iv in Figure 1a). After template removal by calcination (Step 4 in Figure 1a), the imprinted hierarchically ordered macro-meso-microporous structures constructed by zeolite nanocrystals (denoted as OMMM-ZSM-5(*x*). OMMM represents ordered macro-meso-microporous zeolite, where *x* represents the macropore size of OMMM-ZSM-5 zeolites, *x* =200, 400 and 600) were obtained (v in Figure 1a).

Scanning electron microscope (SEM) images show that OMMM-ZSM-5(400), as a representative sample has a highly ordered three-dimensional inverse opal macroporous structure with an excellent regular periodicity (Figure 1b). The ordered hexagonally arrayed cages of about 400 nm are interconnected by windows of 100 nm (Figure 1c, 1d). The walls shared by two adjacent macropores are completely constructed by uni-sized zeolite spheric nanocrystals of 20 nm (Figure 1e and f)

7

corresponding exactly to the size of original amorphous SiO_2 spheres used as silica precursor. High-resolution (HR) TEM studies display that these nanospheres are pure zeolite ZSM-5 nanocrystals with high crystallinity and uniform particle size of 20 nm (Figure 1f and g) in excellent agreement with SEM observation. These mono-disperse zeolite nanocrystals are densely packed to form ordered mesoporous interstitial voids (Figure 1g). A strong diffraction peak can be found in the small-angle X-ray diffraction pattern (Figure 1h), evidencing clearly the formation of the highly ordered mesostructure of the OMMM-ZSM-5(400). The wide-angle X-ray diffraction pattern of OMMM-ZSM-5(400) (Figure 1i) further confirms the formation of a pure MFI zeolite phase with high crystallinity. The presence of micro- and mesopores in OMMM-ZSM-5(400) is further certified by nitrogen adsorption-desorption isotherms (Figure 1j). OMMM-ZSM-5(400) shows a micropore size distribution centered at 0.5 nm on the basis of the NLDFT (Nonlocal density functional theory) method, which is from the micropores of ZSM-5 zeolite. The micropore surface area and volume of OMMM-ZSM-5(400) are 163 m^2g^{-1} and 0.09 cm^3g^{-1} (Table S1), respectively. The hysteresis loop observed in the isotherms corresponds to the abundant mesopores with the mesopore size distribution centered at 8 nm. This pore size exactly corresponds to the interstitial diameter of the close packed zeolite nanocrystals. The BET surface area and total pore volume of OMMM-ZSM-5(400) are 434 m^2g^{-1} and 0.3 cm^3g^{-1} (Table S1), respectively. The presence of meso- and macropores in OMMM-ZSM-5(400) is further illustrated by mercury intrusion porosimetry measurement (Figure S1). The OMMM-ZSM-5(400) shows a mesopore distribution centered at ~7.2 nm, practically

8

same as the value obtained by the N_2 adsorption, and a narrow macroporous distribution centered at ~100 nm corresponding to the window size of the macroporous cage. Due to the technique limit, the larger microporous cages of 400 nm observed by SEM (Figure 1b, c and d) and TEM (Figure 1e) are not seen by mercury intrusion porosimetry. The ^{29}Si MAS NMR spectrum of OMMM-ZSM-5(400) shows a highly intense resonance at -114 ppm and a shoulder at -106 ppm, indicating that the framework consisted primarily of crosslinked Q^4 silica units [δ=-110 ppm, -114 ppm, -118 ppm, $Si(OSi)_4$] and Q^3 silica units [δ=-102 nm, $Si(OSi)_3(OH)$] (Figure S2a). The ^{27}Al MAS NMR spectrum (Figure S2b) shows that aluminum atoms solely exist in the tetrahedral position ($\delta = 50$ ppm) and no extra-framework aluminum species ($\delta = 0$ ppm) are found, indicating that the amorphous aluminum atoms are all incorporated into the macro-meso-microporous framework in tetrahedral positions after the crystallization transformation process. The characterization data of OMMM-ZSM-5(200) and (600), conventional microszied (C-ZSM-5) and ZSM-5 nanocrystals (Nano-ZSM-5) are given in Figures S3-7).

The generalized Murray's Law (Equation S1) was used to evaluate the hierarchically porous structural characteristics of our OMMM-ZSM-5 zeolites. The different size ratios between multi-scale pores can be expressed by Equations S2 and S3[28]. More insight on the establishment of these equations and the calculations of different pore sizes using these equations can be found in supporting information. On the basis of the average number of micropores in one ZSM-5 spherical nanocrystal of our OMMM-ZSM-5 (Equation S4 and Figure S8), when $D_{micro} = 0.5$ nm (Figure 1j),

9

the optimized diameter of mesopores should be around 10 nm in our OMMM-ZSM-5 (Figures S9, S10 and Equation S2). Mesopores of 8 nm obtained (Figure 1j) meets quite well the size ratios between micro- and meso- pores. According to the generalized Murray's Law (Equation S3 and Figure S10), the macropore size should be 440 nm. The experimental macropore size of the obtained OMMM-ZSM-5(400) is around 400nm (Figure 1), which also very well matches the size ratios between macro- and meso- pores. Two more OMMM catalysts with different macropore sizes (200 nm and 600 nm) were made for a better comparison. Mesopores of 8 nm obtained (Figures S3d and S4d) meet quite well the size ratios between micro- and meso- pores. The different size ratios between multi-scale pores can be expressed by Equations S2 and S3[28]. According to the generalized Murray's Law (Equation S3, Figures S11 and S12), the macropore size should be 146 nm for OMMM-ZSM-5(200) and 812 nm for OMMM-ZSM-5(600). The experimental macropore sizes of the obtained OMMM-ZSM-5(200) and OMMM-ZSM-5(600) are around 200nm and 600nm (Figure S3 and S4), respectively, which fail to match the theoretically predicted and optimized size ratios between macro- and meso- pores made by the generalized Murray's Law.

These results suggest that our OMMM-ZSM-5(400) obeys finely the pore size ratio at micro- and meso- and macro-pore level required by the generalized Murray's Law for optimized mass transport properties while OMMM-ZSM-5(200) and (600) fail to matches exactly meso-macropore size ratio defined by the generalized Murray's Law. All the above results clearly demonstrate that hierarchical Murray zeolites with a high crystallinity and a highly interconnected, three dimensionally ordered

macro-meso-microporous structure assembled by uniform zeolite nanocrystals are obtained.

In order to gain deeper insight into the chemical crystalline transformation process for the formation of hierarchical Murray zeolites, samples at different crystallization times were collected and intensively characterized by a series of techniques. Using OMMM-ZSM-5(400) as a representative sample, SEM images (Figure S5) clearly show that the three dimensional highly ordered macroporous structure can be retained throughout the whole hydrothermal crystallization transformation process. TEM images display the same size of the monodisperse nanospheres in the samples with different crystallization times (Figure 2a-d), suggesting that zeolite nanocrystals are derived from the amorphous silica nanospheres of same size. Strong diffraction peaks are observed in the small-angle X-ray diffraction patterns for all the samples (Figure 2e), indicating that the ordered mesoporous structure constructed from monodisperse nanospheres can be well retained during the crystallization process. The amorphous silica precursors gradually disappear, and the crystallinity of the samples gradually increases, which is confirmed by the development of diffraction peaks corresponding to zeolite MFI structure in the wide-angle XRD patterns (Figure 2f). The XRD profile of the OMMM-ZSM-5(400) reveals that a zeolite MFI structure can be obtained with a high degree of crystallinity after crystallization transformation process of 24 h. These observations are further corroborated with ^{29}Si MAS NMR spectroscopy to follow the transformation of the amorphous silica to zeolite nanocrystals during crystallization process (Figure 2g). As the reaction time increases, the intensity at both δ=-96 nm [Q^2

11

groups, $Si(OSi)_2(OH)_2$] and δ=-102 nm [Q^3 groups, $Si(OSi)_3(OH)$] decreases while that at δ=-110 ppm, -114 ppm, -118 ppm, [Q^4 groups, $Si(OSi)_4$] increases, indicating that the gradually increased crystallinity of resultant zeolitic framework. Moreover, the resonance signals become narrower and no Q^2 units exist in OMMM-ZSM-5(400), suggesting that the Si species are completely transformed from an amorphous to a crystalline framework after hydrothermal reaction of 24 h. For ^{27}Al MAS NMR spectroscopy (Figure 2h), the signal centered at about 0 ppm (octahedral Al) gradually decrease as the crystallization time extends, indicating that the aluminum atoms are progressively incorporated into the zeolitic framework at tetrahedral positions during the crystallization transformation process. Only one sharp, symmetrical signal centered at about 50 ppm is observed in OMMM-ZSM-5(400), which means that the amorphous aluminum atoms in precursor are all incorporated into zeolitic framework at tetrahedral positions. N_2 adsorption-desorption analysis of different samples further confirms the gradual generation of microporosity in the products (Figure 2i, Table S1). The surface area and pore volume of micropores increase gradually with increasing crystallization time (Table S1). The micropore size of 0.5 nm calculated by the NLDFT method corresponds to the pore size of zeolite ZSM-5 (Figure 2j). The mesopore size distributions of samples collected at various crystalline times confirm that the mesopore size remain almost the same during the crystalline process (Figure 2k). It can thus be concluded that the confined crystalline transformation process is a successful strategy to create hierarchical Murray zeolites with a highly interconnected, three

12

dimensionally ordered macro-mesoporous structure assembled by uniform zeolite nanocrystals.

The interconnectivity between pores at different level is essential for a hierarchical Murray structure and was firstly studied by the temperature-dependent hyperpolarized ^{129}Xe nuclear magnetic resonance (HP ^{129}Xe NMR, Figure 3a). For comparison, the conventional microporous ZSM-5 (C-ZSM-5) with a similar Si/Al was used as the reference catalyst (Figure S6). A series of peaks at 0 ppm from 273 K to 153 K are observed in C-ZSM-5 due to the presence of Xe in the gas phase at each temperature. Only one signal, line *A* (116-186 ppm), could be observed in the spectra of C-ZSM-5 from 273 to 153 K (Figure S13), which is ascribed to the Xe adsorbed in the 10-membered ring channel of ZSM-5[15]. For OMMM-ZSM-5(400), the temperature-dependent behavior of line *A* in Figure 3a is the same as that of C-ZSM-5 (Figure S13), indicating that the maintained microporosity in the OMMM-ZSM-5(400). In addition to line *A*, a shoulder of *line B* appears ranging from 120 to 108 ppm at a low temperature from 203 to 173K and the chemical shifts move downfield as temperature decreased. The shoulder and the new upfield *line B* at low temperatures are due to the Xe adsorbed in the mesopores and macropores in OMMM-ZSM-5(400). At a relatively high temperature above 203K, the rapid exchange of Xe between the micropores and the macro-mesopores in OMMM-ZSM-5(400) sample leads to the preferential adsorption of Xe in the micropores rather than in the mesopores and macropores, leading to the disappearance of the signals of *line B*. At high temperature, in addition to the signal corresponding to gas Xe, there is only one signal

13

corresponding to the adsorption in micropores for OMMM-ZSM-5(400), suggesting that there is no other isolated pore and macro-mesoporosity is highly connected with intrinsic microporosity in OMMM-ZSM-5(400). These results very clearly indicate that the excellent interconnectivity of hierarchical Murray structure in OMMM-ZSM-5(400).

Concerning the mass transfer of bulky molecules within the highly interconnected hierarchical Murray structure of OMMM-ZSM-5, the intelligent gravimetric analysis (IGA), a macroscopic diffusion measurement, on the diffusion of 1,3,5-trimethylbenzene (1,3,5-TMB), was performed under inert conditions (Figure 3b, 3c). For a better comparison, the conventional microporous ZSM-5 (C-ZSM-5, Figure S6) containing micro-mesopores and ZSM-5 nanocrystals (Nano-ZSM-5, Figure S7) containing micro-macropores were used as reference catalysts. It is clearly seen that OMMM-ZSM-5 zeolites have much larger max adsorption amounts at any relative pressure (Figures 3b and c) and faster relative diffusion rate than those of C-ZSM-5 and Nano-ZSM-5 (Table S2). This observation is directly linked to the excellent connectivity between micropores and meso-macropores of OMMM-ZSM-5 zeolites. The highest adsorption amounts of 1,3,5-TMB and the highest diffusivity observed for OMMM-ZSM-5 (400) explain its optimized Murray structure. The above results show that the highly ordered and interconnected hierarchically macro-mesoporous structure inside our Murray zeolite is much more effective than micro-macroporous nanocrystals and micro-mesoporous microsized conventional ZSM-5 zeolite. Such unique hierarchically porous architecture can maximize the diffusion rate of reactants and products by reducing effective diffusion length. The pore size ratio obeying the

14

generalized Murray's Law found in OMMM-ZSM-5(400) gives the best diffusion properties compared to two other OMMM-ZSM-5(200) and (600) samples which fail to match the theoretically predicted and optimized size ratios between macro- and meso-pores defined by the generalized Murray's Law. However, thes two samples still present much better diffusion performance than C-ZSM-5 and Nao-ZSM-5 samples (Figure 3b and c) showing the advantage of the introduction of hierarchically micro-meso-macroporous structure into zeolites.

With regard to the intracrystalline diffusion behavior and the impact of the interconnected and rationalized macro-meso-micropores in accelerating diffusion in OMMM-ZSM-5(400) zeolite, the ^{1}H pulsed field gradient (PFG) NMR, a microscopic diffusion measurement, was applied to OMMM-ZSM-5(400) as a representative sample. The methane due to its small size was chosen for these experiments with different loadings of 2.31, 3.70 and 5.13 mmol g^{-1} in OMMM-ZSM-5(400) zeolites over a wide range of diffusion times from 6 to 50 ms at 298 K. More description about the technique (Equations S6-S12) can be found in supporting information. The self-diffusivity D_f is the slope in a semi-logarithmic plot of the PFG NMR signal attenuations versus the squared field-gradient pulse intensity $(\gamma\delta g)^2$. Two independent linear relationships are observed in all the plots (Figure 3c-e). The first and steep decay corresponds to the methane molecules leaving the porous particles and diffusing rapidly in the interparticle space during the diffusion time t, as shown in the first part of Equation S11. The second, more slowly decaying part of the attenuation represents the diffusion of methane strictly confined in the macro-meso-microporous structure

15

during the diffusion time t, as shown in the second part of Equation S11. Here we only consider the mass transfer within the OMMM-ZSM-5(400), i.e., the intracrystalline diffusion. The intracrystalline self-diffusivities ($D_{f\text{-}intra}$) determined from the slope of the second part in the curves for different observation times t are shown in the Figure 3f. Compared to $D_{f\text{-}intra}$ of methane molecules in purely microporous ZSM-5 in the order of 10^{-9} m$^2\cdot$s^{-1}[31], the values of $D_{f\text{-}intra}$ of methane at different loadings in OMMM-ZSM-5(400) are at the order of 10^{-8} m$^2\cdot$s^{-1} which are 10 times higher and mean that mesopores and macropores in OMMM-ZSM-5(400) can highly facilitate the diffusion of methane. The overall diffusion in OMMM-ZSM-5(400) is thus significantly improved. In Figure 3g, we note that the mean squared value of the displacements $r(t)$ significantly exceeds the size of the nanocrystals (~20 nm), indicating that the transfer of the methane molecules through the OMMM-ZSM-5(400) hierarchical porous structure consists of displacements alternating between micro-, meso-, and macropores. The total diffusivity of molecules ($D_{f\text{-}intra}$) in our hierarchical Murray zeolite is composed of the contribution from the diffusivity in micropores ($D_{f\text{-}micro}$), in mesopores ($D_{f\text{-}meso}$) and in macropores ($D_{f\text{-}macro}$). Assuming that the mean lifetimes spent by the diffusing methane molecules within each type of pores is negligibly small compared with the observation time (fast-exchange condition[32]), Equation 1 can be obtained [33,34]:

$$D_{f-intra} = p_{micro}D_{f-micro} + p_{meso}D_{f-meso} + p_{macro}D_{f-macro} \tag{1}$$

in which p_x (x=micro, meso and macro, $p_{micro}+p_{meso}+p_{macro}=1$) is the relative number of molecules in the micro-, meso- and macropores, as defined on the basis of Einstein

16

relation (Equation S8). The diffusivities in the meso- ($D_{f\text{-}meso}$) and macropores ($D_{f\text{-}macro}$), offering much large mean free paths, belong to the Knudsen-type molecular propagation[33,35] and exceed the micropore diffusivities ($D_{f\text{-}micro}$) by at least one order of magnitude[36-38]. The $D_{f\text{-}intra}$ in our OMMM-ZSM-5(400) obtained by ^{1}H PFG NMR is about 10 times higher than for a single microporous zeolite ZSM-5. This diffusion enhancement phenomenon can be directly attributed to the rational and quantitative relationship between macropores, mesopores and micropores in OMMM-ZSM-5(400) which obeys the generalized Murray's Law and their excellent interconnectivity. This is consistent with the HP [129]Xe NMR and IGA results, indicating that such unique hierarchical Muarry architecture can boost the diffusion rate of reactants and products, leading to a much higher utilization efficiency of the active sites within zeolites.

The distribution of active sites is one of the most important factors to determine the catalytic performance. To illustrate the extraordinary accessibility to active sites of OMMM-ZSM-5 zeolites, the acidic properties and the distribution of active sites were determined by the ammonia temperature programmed desorption (NH$_3$-TPD) analysis and the probe molecules (trimethylphosphine oxide TMPO and tributylphosphine oxide TBPO) adsorption method (Table S3), respectively. The TMPO molecule with a kinetic diameter of 0.55 nm can penetrate into 10-membered-ring micropores (0.55 nm) and will give the total acidity of zeolites while the TBPO molecule is sterically bulky with a kinetic diameter of 0.82 nm and can only access the acid sites on the external surface out of micropores[39]. The acid sites constrained within the

17

micropores are named as internal acid sites and all the acid sites out of micropores are external acid sites. The NH_3-TPD profiles (Figure S14) indicate that the acidities in the three OMMM-ZSM-5(*x*) (*x*=200, 400 and 600) are clearly similar with that in the two reference samples with the similar Si/Al ratios, C-ZSM-5 and Nano-ZSM-5 (Table S3). This is because NH_3 is a very small molecule with a molecule size of 0.26 nm and can access to all the cages and channels of ZSM-5 zeolites. The NH_3-TPD gives the total acidities of ZSM-5 zeolites. Their total acidities made by trimethylphosphine oxide (TMPO) analysis are almost the same because the TMPO molecule with a kinetic diameter of 0.55 nm can penetrate into 10-membered-ring micropores (0.55 nm) and give the total acidity of zeolites. However, the external acidity made by large TPBO molecule with a kinetic diameter of 0.82 nm is much higher for OMMM-ZSM-5(*x*) (*x*=200, 400 and 600 (Table S3). Nano-ZSM-5 has an improved adsorption capacity for TBPO (79 $\mu mol \cdot TBPO \cdot g^{-1}$ cat) compared to that of C-ZSM-5 (41 $\mu mol \cdot TBPO \cdot g^{-1}$ cat) due to its larger external surface area. While three OMMM-ZSM-5 sample contains much higher surface acidity sample contains much higher surface acidity. For example, the external surface acidity of OMMM-ZSM-5(400) (124 $\mu mol \cdot TBPO \cdot g^{-1}$ cat) is 3 times higher than that of C-ZSM-5 and 30% higher than Nano-ZSM-5, respectively. These increased catalytic sites within the OMMM-ZSM-5 catalysts are owing to their widely-open framework, which are of great importance for the catalytic performance.

The synergy of excellent diffusion property and the abundant accessible acid sites makes hierarchical Murray zeolite ZSM-5 an extraordinary solid acid catalyst, especially for converting large organic molecules. The catalytic performances were evaluated in the

18

cracking reaction of bulky 1,3,5-triisopropylbenzene (1,3,5-TIPB) to check the impact of improved diffusion properties. 1,3,5-TIPB molecules have larger kinetic molecular diameters (0.95 nm) than the pore opening of the zeolite ZSM-5 (0.55 nm) and thus are commonly used to study the external surface properties of different zeolites. The microsized ZSM-5 (C-ZSM-5) and the nanosized ZSM-5 (Nano-ZSM-5) have been used as reference catalysts. The pore size distributions are added in Figures S6c and S7c to have a clear understanding of the effectiveness of mesopores and macropores. The N_2 adsorption-desorption isotherms (Figures S6c and S7c) show clearly that the C-ZSM-5 has mesopores at 2 nm and the Nano-ZSM-5 has macropores around 50 nm. These two samples containing hierarchically multiple porosity (micro-mesopores for C-ZSM-5 and micro-macropores for Nano-ZSM-5) are thus excellent references for comparison with our micro-meso-macroporous Murray zeolites.

The changes of both 1,3,5-TIPB conversion and the associated product selectivity with time-on-stream are reported in Figure 4. At each reaction time, C-ZSM-5 and theNano-ZSM-5 give very low and medium conversion, respectively. In contrast, OMMM-ZSM-5 catalysts are most active. For more accurately estimating their catalytic activity, the turnover number (TON) values, normalized by the acidity amount of different catalysts, were shown in Table S5[40]. Clearly, the TON of all three OMMM-ZSM-5s at reaction time of 1h to 8h are much higher than those of C-ZSM-5 and Nano-ZSM-5. This observation is directly linked to the excellent connectivity between micropores and meso-macropores of OMMM-ZSM-5 zeolites. Notably, for OMMM-ZSM-5(400), the TON value was 0.126 at time on stream of 8h, which are 10-fold and 3-fold higher compared to those of C-ZSM-5 and Nano-ZSM-5, respectively. At

each reaction time, OMMM-ZSM-5(400) has the highest TON compared to that of OMMM-ZSM-5(200) and OMMM-ZSM-5(600). The highest TON observed for OMMM-ZSM-5 (400) is attributed to its optimized structure which fully obeys the generalized Murray's Law. On the other hand, the product distribution provides the information about the extent of cracking degree. The deep cracking of 1,3,5-TIPB takes three successive steps, which are the first dealkylation of 1,3,5-TIPB to form diisopropylbenzene (DIPB) and propylene, the second dealkylation of DIPB to give isopropylbenzene (IPB) and propylene and the third dealkylation of IPB to give benzene (Bz) and propylene[41]. The main products catalyzed by C-ZSM-5 are propylene and DIPB accompanied by few IPB and benzene, indicating the low cracking degree of 1,3,5-TIPB. The DIPB content increases with the reaction time (Figure 4b), suggesting the decreased cracking ability of C-ZSM-5. The interparticular mesopores in Nano-ZSM-5 offer better accessibility to external active sites and facilitates the diffusion of the bulky 1,3,5-TIPB as compared with C-ZSM-5 (Figure 4c). The same decreasing trend of cracking ability with increasing reaction time is observed for Nano-ZSM-5. Significantly, the selectivity for the deep cracking products over OMMM-ZSM-5 is much higher than those of C-ZSM-5 and Nano-ZSM-5 when compared at the same reaction time (Figure 4d). The main products for OMMM-ZSM-5 are benzene and propylene with few contents of DIPB, indicating the much deeper cracking degree of 1,3,5-TIPB over OMMM-ZSM-5 catalysts. The selectivity for the deep cracking products (Propene and benzene) over OMMM-ZSM-5(400) with optimized Murray structure is higher than those of OMMM-ZSM-5(200) and OMMM-ZSM-5(600) at the same reaction time (Figure 4d). To compare the selectivity of the five catalysts at the equal conversion, the

20

weight hourly space velocity (WHSV) was adjusted so as to obtain similar 1,3,5-TIPB

conversions around 32% at 280 °C, with the data shown in Table S4. OMMM-ZSM-5(400)

gave a very high selectivity for benzene product of 20.3 % that is obviously higher than the

other four catalysts. This result demonstrates that hierarchical Murray zeolites with optimized

structural feature can substantially promote the selectivity for deep-cracking product in

cracking of 1,3,5-TIPB. It is worthy noting that although OMMM-ZSM-5(400) obeying

exactly the generalized Murray's Law, OMMM-ZSM-(5(200) and (600) still present much

better catalytic properties than C-ZSM-5 and Nao-ZSM-5. Considering the similar total

acidity of the three OMMM-ZSM-5(x) (x=200, 400 and 600) and the two reference samples

(C-ZSM-5 and Nano-ZSM-5), their high deep-cracking performances are attributed to the

introduction of the fully interconnected hierarchically micro-meso-macroporous structures.

The deeper cracking process and higher catalytic stability of three OMMM-ZSM-5

catalysts than those of C-ZSM-5 and Nano-ZSM-5 should be attributed to their significant

diffusion performance of bulky molecules and their low amount of coke deposition. The coke

deposition on the reacted samples was analyzed by the thermogravimetric analysis (TGA,

Table S6). OMMM-ZSM-5(400) used in cracking of 1,3,5-TIPB for 8h shows two times and

30% less coke deposition (6.7 %) than C-ZSM-5 (13.3 %) and Nano-ZSM-5 (9.4 %). It is

clear that the presence of excellent hierarchical Murray structural diffusion system and strong

accessible external surface acidity provides a highly efficient catalyst, exhibiting enhanced

catalytic activity, deep cracking ability as well as higher coke resistance in the 1,3,5-TIPB

catalytic cracking. Consequently, such hierarchically ordered macro-meso-microporous

Murray zeolite is the promising catalyst in many organic catalytic reactions involving large molecules.

In conclusion, the hierarchical Murray zeolite with highly ordered and fully interconnected macro-meso-microporous structure is successfully prepared via a hydrothermal chemical transformation process. Such novel Murray structure has a rational and quantitative relationship between macropores, mesopores and micropores according to the generalized Murray's Law. The resultant hierarchical Murray zeolites exhibit excellent mass transport properties and thus consequently superior catalytic performance in the cracking of bulky 1,3,5-triisopropylbenzene. The generalized Murray's Law could enable predictable and controlled production of bioinspired hierarchically porous materials with optimized structural features and highly enhanced performance.

MATERIALS AND METHODS

Synthesis of polystyrene spheres (about 420nm)

In a typical synthesis, 47 g styrene was added in 400g deionized H_2O followed by adding 0.43 g potassium persulfate. The reaction was performed at 80°C for 5 h in an argon atmosphere.

Synthesis of Hierarchically ordered polystyrene-silica-carbon composites

In a typical procedure[42], the as-synthesized polystyrene nanospheres were first blended with silica sol (LUDOX AS-40 colloidal silica, 40 wt.% suspension in water, average particle size is 22 nm, Sigma-Aldrich) under magnetic stirring for 1 h to obtain

22

nanocomposite colloidal and then with sucrose at room temperature for 10 min, followed by the addition of sulfuric acid (95.0-98.0 wt. % in water, sinoreagent) under stirring for another 10 min to obtain a stable dispersion. The typical mass ratio of polystyrene nanospheres, silica nanospheres, sucrose, and sulfuric acid was 100:15:15:1.5. The as-prepared dispersion was directly dried in an oven at 110°C for 6 h, then at 160°C for 6 h.

Synthesis of hierarchically ordered macro-meso-microporous ZSM-5 nanocrystals

Polystyrene-silica-carbon composites were impregnated with an aqueous solution containing aluminum sodium oxide (NaAlO$_2$, 99.99 % metal basis, aladin) and tetrapropylammonium hydroxide (TPAOH, 1M in water, aladin). Then the mixture was stirred for 1h and transferred to the vacuum system and undergo rotary evaporation at 60°C to make sure there only existed trace amount of water. The mixture was transferred to the autoclave under 130°C for a certain time. The products were washed with distilled water, dried in air at 60°C and finally calcined at 550°C for 7 h to remove the templates. The as-synthesized samples are denoted by OMMM-ZSM-5.

Commercial microporous ZSM-5 (C-ZSM-5) and ZSM-5 zeolite nanocrystals (Nano-ZSM-5) from FUYU New Materials Technology Co., Ltd. were used as reference samples.

Catalyst Characterization

Small-angle X-ray scattering (SAXS) and wide-angle X-ray scattering (WAXS) measurements of solid samples were taken on a Bruker D8 Advance diffractometer with CuKα monochromatized radiation (λ =1.5418 Å).

Scanning electron microscope (SEM) images were obtained on a Hitachi S4800 field-emission SEM operated at 5 kV and 10 μA. Transmission electron microscope (TEM) images were performed on a Thermo Fisher Titan Themis 60-300 'cubed' microscope fitted with double aberration-correctors, operated at 120 kV.

The chemical composition of the samples was determined by inductively coupled plasma optical emission spectroscopy (ICP-OES) using a PerkinElmer Optima 4300DV.

N_2 adsorption-desorption isotherms were measured using a Micrometrics ASAP 2020 gas sorptometer after the samples were degassed at 573K under vacuum for 12h.

The NMR spectra were recorded at room temperature, using a Varian VNMRS spectrometer operating at 9.4 T (^{27}Al freq. = 79.46 MHz; ^{29}Si freq = 79.46 MHz). The samples were packed in a standard 4mm rotor and spun at 10 kHz. For ^{27}Al, the parameters were: spectral width about 104 kHz, relaxation delay 100 ms, excitation pulse 3 us, acquisition time 5 ms. For ^{29}Si, the parameters were: spectral width of about 104 kHz, relaxation delay 6 ms, excitation pulse 3 us, acquisition time 5 ms.

Laser hyperpolarized ^{129}Xe NMR experiments was used to investigate the interconnectivity between macropore, mesopore and micropore. Both 1,3,5-trimethylbenzene diffusion measurement in ZSM-5 zeolites was performed on a

24

computer-controlled intelligent gravimetric analyzer (IGA, Hiden Analytical Ltd., Warrington, UK), a macroscopic diffusion measurement, and the ^{1}H pulsed field gradient (PFG) NMR, a microscopic diffusion measurement, were applied to investigate the intracrystalline diffusion and the impact of the interconnected macro-meso-micropores in accelerating diffusion in zeolites. The details can be found in supporting information.

The catalytic performances were evaluated in the cracking reaction of bulky 1,3,5-triisopropylbenzene (1,3,5-TIPB). The details can be found in supporting information.

25

AUTHOR CONTRIBUTIONS

L. H. Chen and B. L. Su conceived the project; L. H. Chen and B. L. Su supervised the study; M. H. Sun designed and performed experiments, characterized samples, analyzed data and wrote the draft of the manuscript. S. S. Gao and S. T. Xu performed the diffusion test and analyzed the diffusion data. Z. Y. Hu performed TEM microscopy analysis. T. Barakat, Z. Liu, S. Yu, J. M. Lyu and Y. Li performed the characterizations of samples. L. H. Chen wrote the manuscript. L. H. Chen and B. L. Su revised the manuscript and finalized the manuscript.

Conflict of interest statement. None declared.

26

REFERENCE

1. Schneider D, Mehlhorn D and Zeigermann P *et al.* Transport properties of hierarchical micro-mesoporous materials. *Chem Soc Rev* 2016; **45**: 3439-67.

2. Chen L-H, Sun M-H and Wang Z *et al.* Hierarchically structured zeolites: From design to application. *Chem Rev* 2020; **120**: 11194–294.

3. Zhou J, Fan W and Wang Y *et al.* The essential mass transfer step in hierarchical/nano zeolite: surface diffusion. *Natl Sci Rev* 2019; **7**: 1630-2.

4. Li K, Valla J and Garcia-Martinez J. Realizing the commercial potential of hierarchical zeolites: New opportunities in catalytic cracking. *ChemCatChem* 2014; **6**: 46-66.

5. Schwieger W, Machoke AG and Weissenberger T *et al.* Hierarchy concepts: classification and preparation strategies for zeolite containing materials with hierarchical porosity. *Chem Soc Rev* 2016; **45**: 3353-76.

6. Peng P, Gao X-H and Yan Z-F *et al.* Diffusion and catalyst efficiency in hierarchical zeolite catalysts. *Natl Sci Rev* 2020; **7**: 1726-42.

7. Hartmann M, Machoke AG and Schwieger W. Catalytic test reactions for the evaluation of hierarchical zeolites. *Chem Soc Rev* 2016; **45**: 3313-30.

8. Verboekend D, Nuttens N and Locus R *et al.* Synthesis, characterisation, and catalytic evaluation of hierarchical faujasite zeolites: milestones, challenges, and future directions. *Chem Soc Rev* 2016; **45**: 3331-52.

9. Sun M-H, Huang S-Z and Chen L-H *et al.* Applications of hierarchically structured porous materials from energy storage and conversion, catalysis, photocatalysis, adsorption, separation, and sensing to biomedicine. *Chem Soc Rev* 2016; **45**: 3479-563.

10. Yang X-Y, Chen L-H and Li Y *et al.* Hierarchically porous materials: Synthesis strategies and structure design. *Chem Soc Rev* 2017; **46**: 481-558.

11. Mehlhorn D, Inayat A, Schwieger W *et al.* Probing mass transfer in mesoporous Faujasite-type zeolite nanosheet assemblies. *ChemPhysChem* 2014; **15**: 1681-86.

12. Yutthalekha T, Wattanakit C and Warakulwit C *et al.* Hierarchical FAU-type zeolite nanosheets as green and sustainable catalysts for benzylation of toluene. *J Clean Prod* 2017; **142**: 1244-51.

13. Gueudré L, Milina M and Mitchell S *et al.* Superior mass transfer properties of technical zeolite bodies with hierarchical porosity. *Adv Func Mater* 2014; **24**: 209-19.

14. Mitchell S, Michels NL and Kunze K *et al.* Visualization of hierarchically structured zeolite bodies from macro to nano length scales. *Nat Chem* 2012; **4**: 825-31.

15. Sun M-H, Zhou J and Hu Z-Y *et al.* Hierarchical zeolite single-crystal reactor for excellent catalytic efficiency. *Matter* 2020; **3**: 1226-45.

16. Na K, Jo C and Kim J *et al.* Directing zeolite structures into hierarchically nanoporous architectures. *Science* 2011; **333**: 328-32.

17. Dai H, Shen Y and Yang T *et al.* Finned zeolite catalysts. *Nat Mater* 2020; **19**: 1074–80.

18. Li B, Hu ZJ and Kong B *et al.* Hierarchically tetramodal-porous zeolite ZSM-5 monoliths with template-free-derived intracrystalline mesopores. *Chem Sci* 2014; **5**: 1565-73.

19. Hung C-T, Duan L and Zhao T *et al.* Gradient Hierarchically Porous Structure for Rapid Capillary-Assisted Catalysis. *J Am Chem Soc* 2022; **144**: 6091-99.

20. Jia LY, Raad M and Hamieh S *et al.* Catalytic fast pyrolysis of biomass: superior selectivity of hierarchical zeolites to aromatics. *Green Chemistry* 2017; **19**: 5442-59.

21. Bai R, Song Y and Li Y *et al.* Creating hierarchical pores in zeolite catalysts. *Trends Chem* 2019; **1**: 601-11.

22. Kerstens D, Smeyers B and Van Waeyenberg J *et al.* State of the Art and Perspectives of Hierarchical Zeolites: Practical Overview of Synthesis Methods and Use in Catalysis. *Adv Mater* 2020; **32**: 2004690.

23. Mitchell S, Pinar AB and Kenvin J *et al.* Structural analysis of hierarchically organized zeolites. *Nat Commun* 2015; **6**: 8633.

24. Milina M, Mitchell S and Crivelli P *et al.* Mesopore quality determines the lifetime of hierarchically structured zeolite catalysts. *Nat Commun* 2014; **5**: 3922.

25. Hartmann M, Thommes M and Schwieger W. Hierarchically-Ordered Zeolites: A Critical Assessment. *Adv Mater Interfaces* 2021; **8**: 2001841.

26. Pérez-Ramírez J, Verboekend D and Bonilla A *et al.* Zeolite catalysts with tunable hierarchy factor by pore-growth moderators. *Adv Funct Mater* 2009; **19**: 3972-79.

27. Painter PR, Edén P and Bengtsson H-U. Pulsatile blood flow, shear force, energy dissipation and Murray's Law. *Theor Biol Med Model* 2006; **3**: 31.

28. Zheng X, Shen G and Wang C *et al.* Bio-inspired murray materials for mass transfer and activity. *Nat Commun* 2017; **8**: 14921.

29. Chen L-H. Hierarchically porous materials and green chemistry-an interview with Ming-Yuan He. *Natl Sci Rev* 2020; **7**: 1759-61.

30. Chen L-H, Li Y and Su B-L. Hierarchy in materials for maximized efficiency. *Natl Sci Rev* 2020; **7**: 1626-30.

31. Caro J, Bulow M and Schirmer W *et al.* Microdynamics of methane, ethane and propane in ZSM-5 type zeolites. *J. Chem. Soc., Faraday Trans. I,* 1985; **81**: 2541-2550.

32. Kärger J, Ruthven DM and Theodorou DN. Diffusional effects in zeolite catalysts. *Diffusion in Nanoporous Materials*, 2012, 807-37.

33. Kärger J and Valiullin R. Mass transfer in mesoporous materials: the benefit of microscopic diffusion measurement. *Chem Soc Rev* 2013; **42**: 4172-97.

34. Zeigermann P, Naumov S and Mascotto S *et al.* Diffusion in hierarchical mesoporous materials: Applicability and generalization of the fast-exchange diffusion model. *Langmuir* 2012; **28**: 3621-32.

35. Petropoulos JH and Papadokostaki KG. May the Knudsen equation be legitimately, or at least usefully, applied to dilute adsorbable gas flow in mesoporous media? *Chem Eng Sci* 2012; **68**: 392-400.

36. Kärger J and Volkmer P. Comparison of predicted and nuclear magnetic resonance zeolitic diffusion coefficients. *J Chem Soc, Faraday Trans 1* 1980; **76**: 1562-68.

37. Mehlhorn D, Valiullin R and Kärger J *et al.* Exploring the hierarchy of transport phenomena in hierarchical pore systems by NMR diffusion measurement. *Micropor Mesopor Mat* 2012; **164**: 273-9.

38. Mehlhorn D, Valiullin R and Kärger J *et al.* Intracrystalline diffusion in mesoporous zeolites. *ChemPhysChem* 2012; **13**: 1495-99.

39. Zhao Q, Chen WH and Huang SJ *et al.* Discernment and quantification of internal and external acid sites on zeolites. *J Phys Chem B* 2002; **106**: 4462-69.

40. Zhao Y, Zhang Y and Ding Y *et al.* Hexagonal nanoplates of NiO/CoO/Fe2O3 composite acting as an efficient photocatalytic and electrocatalytic water oxidation catalyst. *Dalton Transactions* 2015; **44**: 15628-35.

41. Sun M-H, Chen L-H and Yu S *et al.* Micron-sized zeolite Beta single crystals featuring intracrystal interconnected ordered macro-meso-microporosity displaying superior catalytic performance. *Angew Chem Int Ed* 2020; **59**: 19582-91.

42. Zhang S, Chen L and Zhou S *et al.* Facile Synthesis of Hierarchically Ordered Porous Carbon via in Situ Self-Assembly of Colloidal Polymer and Silica Spheres and Its Use as a Catalyst Support. *Chemistry of Materials* 2010; **22**: 3433-3440.

Figure Captions
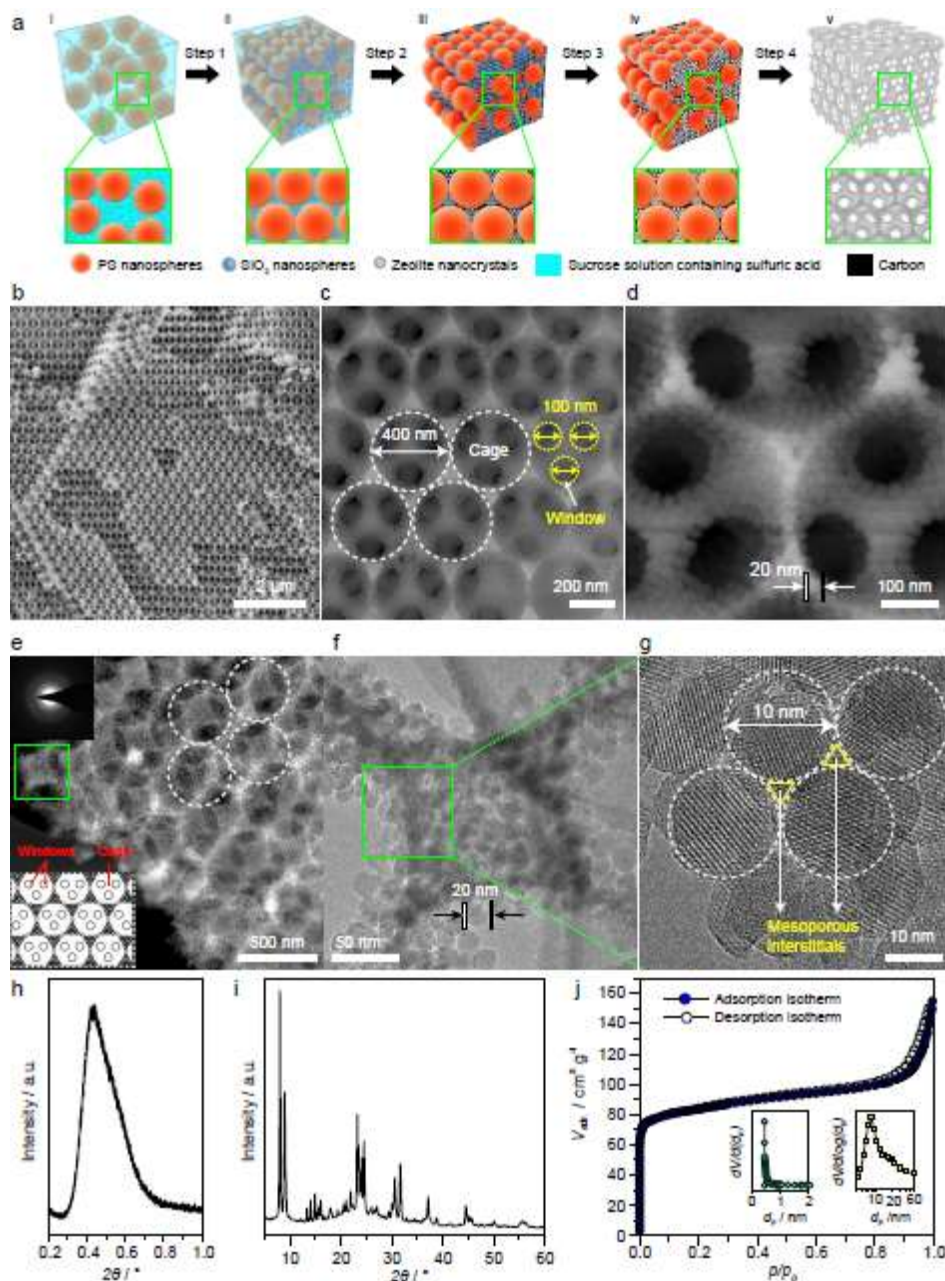
Figure 1 (a) Schematic of the synthesis of hierarchically ordered macro-meso-microporous zeolite ZSM-5 (OMMM-ZSM-5) assembled by zeolite nanocrystals. Steps: 1) Self-assembly, 2) Carbonization, 3) Hydrothermal crystallization and 4) Template removal by calcination. i) Monodispersed polystyrene (PS) nanospheres and SiO_2 nanospheres in sucrose solution, ii) Three dimensionally periodic close-packed PS/SiO_2 spheres in sucrose solution, iii) PS/SiO_2/carbon matrix, iv) PS/ZSM-5 zeolite nanocrystals/carbon matrix and v) OMMM-ZSM-5 by template removal via calcination. (b-j) Characterizations of OMMM-ZSM-5(400), as a representative sample. (b-d) SEM images. (e) TEM image and ED pattern (inset). (f) TEM image of enlarged area outlined in (e), (g) HRTEM image of enlarged area outlined in (f). (h) SAXS and (i) WAXS pattern, (j) N_2 adsorption-desorption isotherms and micropore-size, mesopore-size distribution (inset).

29
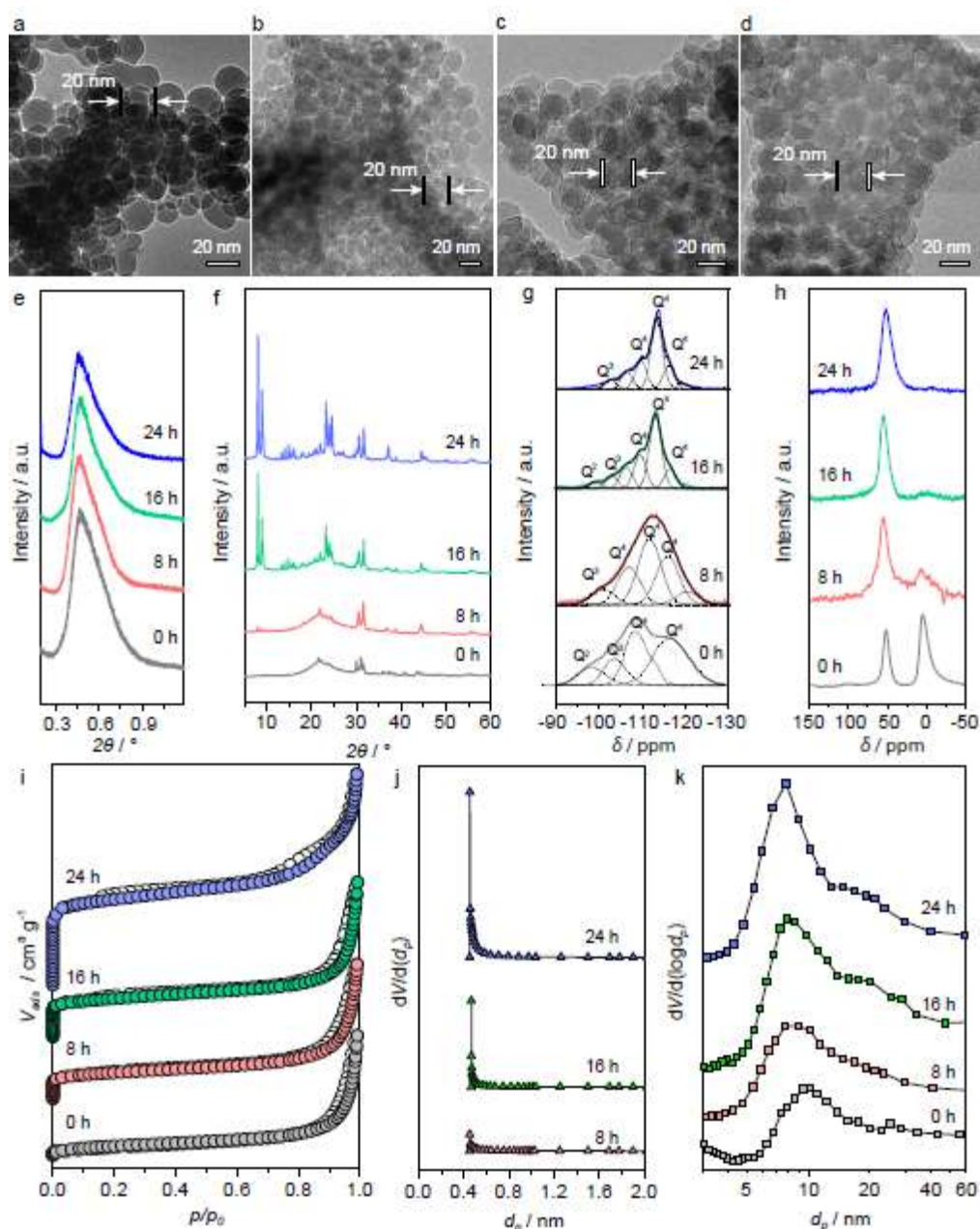
Figure 2 Crystallization process of OMMM-ZSM-5(400). TEM images of OMMM-ZSM-5(400) obtained at (a) 0h, (b) 8h, (c) 16h and (d) 24h. (e) SAXS data, (f) WXAS data, (g) ^{29}Si NMR spectra (the black plots are the fitted data), (h) ^{27}Al NMR spectra and (i) nitrogen adsorption isotherms, (j) micropore size distributions and (k) mesopore size distributions
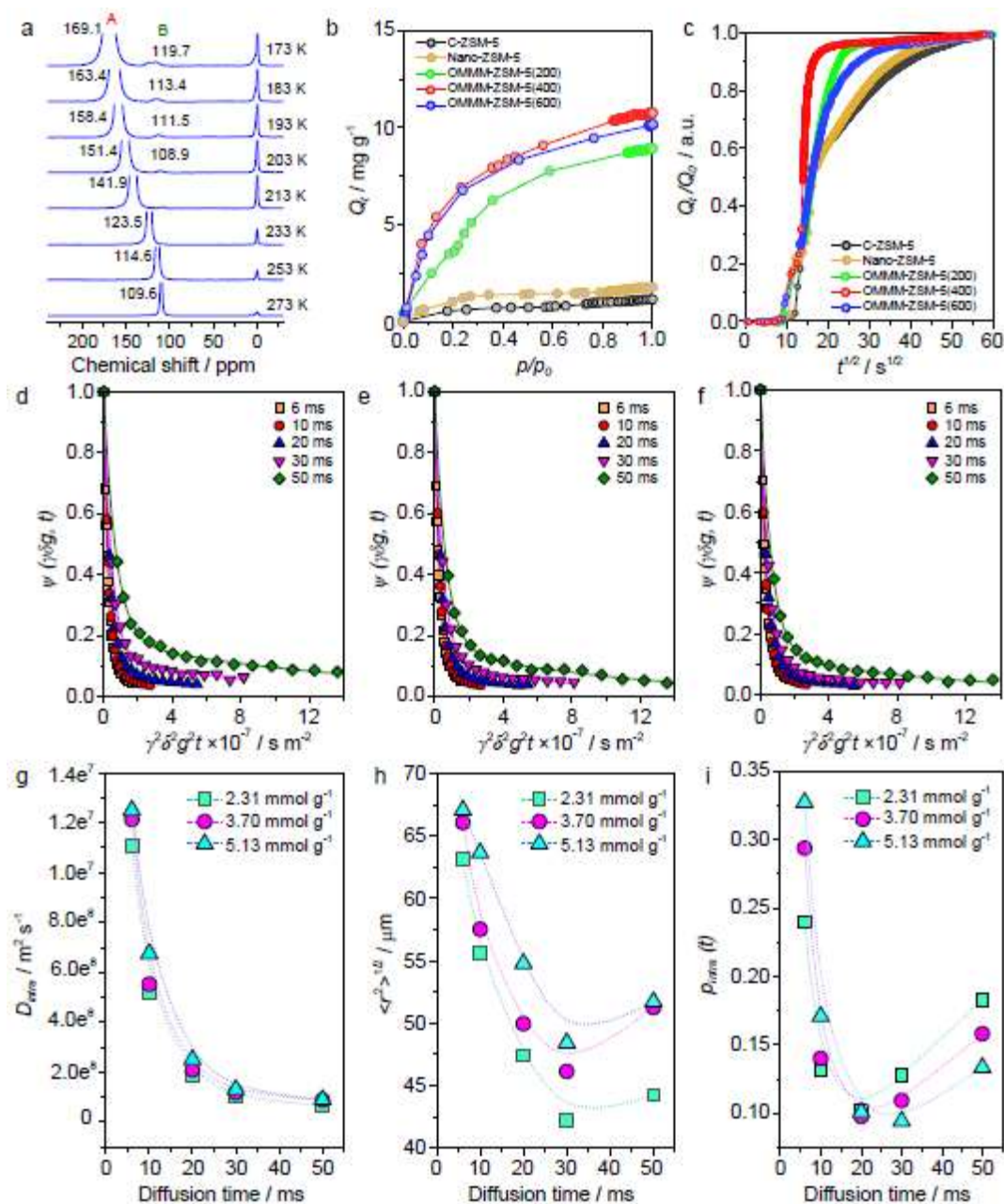
Figure 3 (a) Laser-hyperpolarized ^{129}Xe NMR spectra with temperature varied from 273 K to 173 K of OMMM-ZSM-5(400). (b, c) The macroscopic diffusion measurement. Adsorption and diffusion performance of 1,3,5-TMB within ZSM-5 samples. (b) The isothermal adsorption curve, (c) Normalized uptake (Q_t/Q_0) profiles of 1,3,5-trimethylbenzene over different catalysts. (d-h) The microscopic diffusion measurement. (d-f) ^{1}H PFG NMR attenuation curves for methane with loading of (d) 2.31 mmol·g^{-1}, (e) 3.7 mmol·g^{-1} and (f) 5.13 mmol·g^{-1} in OMMM-ZSM-5(400) for different observation/diffusion times t measures at 298K. (g) Intracrystalline diffusivities $D_{f\text{-}intra}$, (h) the mean squared value of the displacements $<r^2>^{1/2}$ and (i) the relative number of methane molecules still within OMMM-ZSM-5(400) $p_{intra}(t)$ of methane with different loadings in OMMM-ZSM-5(400) determined from PFG NMR attenuation curves in (d-f).

31
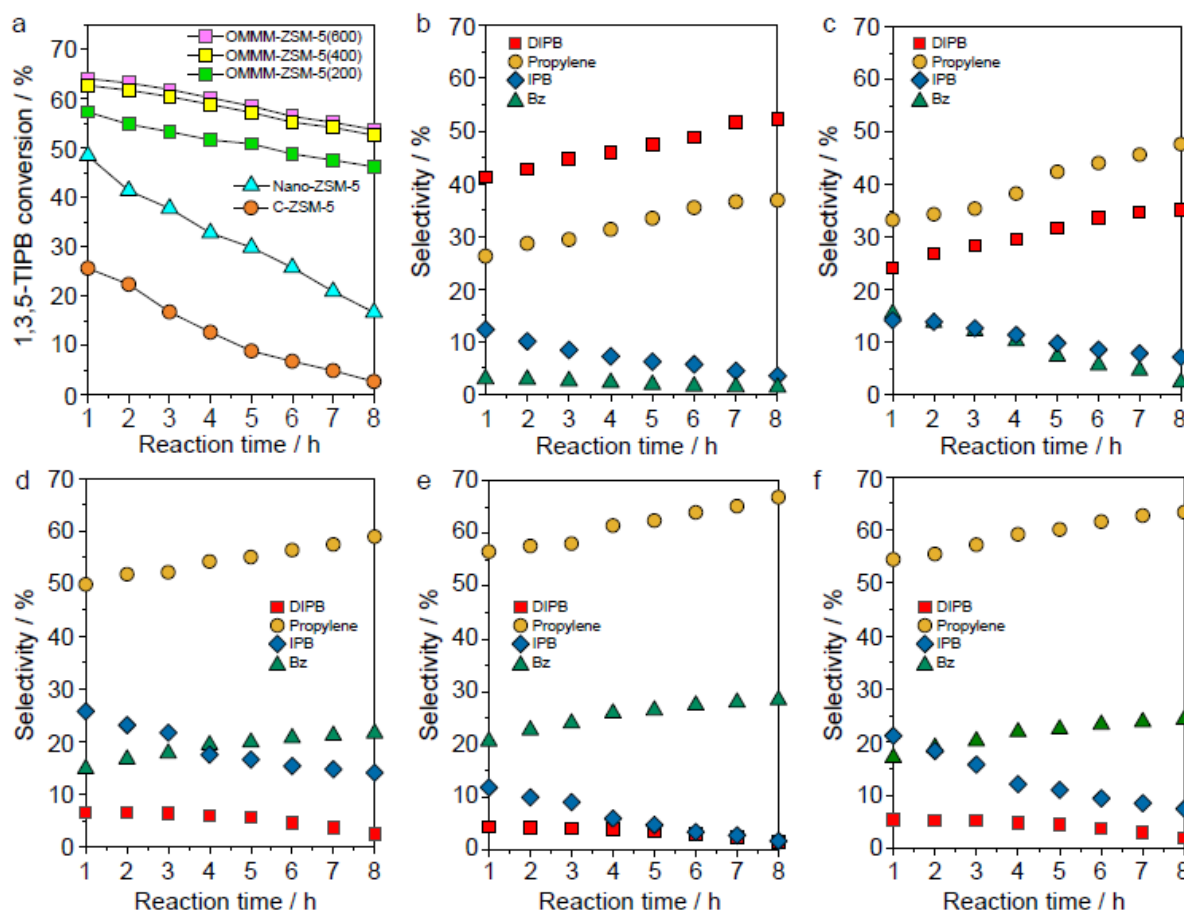
Figure 4 Catalytic performance of various zeolite ZSM-5 catalysts in the cracking reaction of 1,3,5-TIPB (a) catalytic activities (1,3,5-TIPB conversions) at different reaction time. (b-e) The product distributions in the 1,3,5-TIPB cracking using (b) C-ZSM-5, (c) Nano-ZSM-5, (d) OMMM-ZSM-5(200), (e) OMMM-ZSM-5(400) and (f) OMMM-ZSM-5(600).